Experimental investigation of the amplitudes of the quantum oscillations in the transport coefficients of Al

R. Fletcher
Physics Department, Queen's University, Kingston, Ontario K7L 3N6, Canada
(Received 21 March 1983)

Absolute measurements on the quantum oscillations in the transverse resistivity (both thermal and electrical) and the thermopower of Al have been made at fields of up to 8 T in the liquid-helium temperature range. The results show that the oscillations are related by known factors to a precision of a few percent. The agreement between theory and experiment suggests that phonon drag plays no observable role in the thermoelectric oscillations. There is an unresolved problem of precisely how the many-body effects are incorporated in the theory, though this does not affect the conclusions of this investigation in any way.

I. INTRODUCTION

In a previous publication[1] a relationship was established relating the amplitudes of the quantum oscillations in the thermopower to those in the electrical resistivity using a phenomenological model suggested by Young.[2] It was tested using existing experimental results[1] and found to hold to within the accuracy of the various data ($\sim\pm 10$–50%). The main purpose of the present paper is to experimentally investigate the validity of the relationship in the case of Al with an accuracy of the order of 1%. The oscillations in the thermal resistivity have also been examined to complete the set of experimental data on the transverse coefficients.

Al was chosen because of the occurrence of relatively large amplitude oscillations in all the coefficients when the magnetic field is close to a [001] axis (Refs. 3 and 4 give extensive references to earlier experiments). The high Debye temperature of Al is also a useful attribute in that inelastic electron-phonon scattering is weak throughout the liquid-^{4}He temperature range and, as will be discussed in Sec. II, elastic scattering is a prerequisite if the theory is to be tested as accurately as possible. Finally, the low frequency of the oscillations allows a precise test of the predicted phase relationships to be made.

On the other hand, it is known that the amplitude of the oscillations grows rapidly for slight misalignments of $\vec{B}$ from [001] (typically 0.5°) because of the influence of the open orbits that are produced by the asymmetry.[3,4] Under these conditions the sample no longer exhibits the symmetry properties expected for $\vec{B}$ parallel to [001], and the theory must be extended to arbitrary crystal directions: This is done in Sec. II. Using the same model, a simple relationship relating the amplitudes of the oscillations in the electrical and thermal resistivities is also derived.

II. THEORY

The intent of this section is to derive relationships between the various observable oscillatory transport coefficients. As usual one begins with the assumption of a linear relationship between the fluxes and forces as embodied in the generalized Ohm's law

$$\begin{aligned}\vec{J}&=\sigma\vec{E}+\epsilon''\vec{\nabla}T\ ,\\ \vec{U}&=-\pi''\vec{E}-\lambda''\vec{\nabla}T\ ,\end{aligned}\tag{1}$$

where $\vec{J}$ and $\vec{U}$ are the electric and thermal current densities, σ and λ'' are the electric thermal conductivity tensors, and ϵ'' and π'' are the thermoelectric and Peltier tensors. We shall denote monotonic quantities by an overbar and oscillatory quantities by a tilde, e.g., $\sigma=\bar{\sigma}+\tilde{\sigma}$.

It is convenient to first examine the expected relationship between the measured electrical and thermal resistivities ρ and γ; we assume throughout that $\rho=\sigma^{-1}$ and $\gamma=\lambda''^{-1}$, i.e., we assume that ρ is measured isothermally and that the thermoelectric correction to γ is negligible. By definition we have $\sigma\rho=1=(\bar{\sigma}+\tilde{\sigma})(\bar{\rho}+\tilde{\rho})$. Since $\bar{\sigma}\bar{\rho}=1$ then $\sigma\tilde{\rho}=-\tilde{\sigma}\bar{\rho}$ and similarly $\lambda''\tilde{\gamma}=-\tilde{\lambda}''\bar{\gamma}$. Using Young's result[1,2] that

$$\tilde{\lambda}''=[-3D''(X)/D(X)]L_0T\tilde{\sigma}=\alpha L_0T\tilde{\sigma}\ ,$$

where L_0 is the Sommerfeld value of the Lorenz number, $D(X)=X/\sinh X$, $D''(X)=d^2D(X)/dX^2$, $X=2\pi^2kTm^*/\hbar eB$ with usual symbols, and assuming the validity of the Wiedemann-Franz law for the monotonic parts, i.e., $\bar{\lambda}''=L_0T\bar{\sigma}$ (so that $\bar{\gamma}L_0T=\bar{\rho}$), then we have

$$\lambda''\tilde{\gamma}=-\alpha\tilde{\sigma}\bar{\rho}=\alpha\sigma\tilde{\rho}\ .$$

Providing $\tilde{\lambda}''\ll\bar{\lambda}''$ and $\tilde{\sigma}''\ll\bar{\sigma}$, then λ'' and σ can be replaced by $\bar{\lambda}''$ and $\bar{\sigma}$ to give the required result

$$\tilde{\gamma}L_0T=\alpha\tilde{\rho}\ .\tag{2}$$

The last assumption is not particularly restrictive in these experiments. As $X\to 0$, $\alpha\to 1$ (in fact by $X=0.5$, α is already 0.87). For the present experiments $X=1.27T/B$ with B in the range 4–8 T and T between 1.7 and 3.8 K. We see that $\alpha\sim 1$ and to assume $\lambda''=L_0T\sigma$ should be an excellent approximation. The worst case conditions correspond to low B and high T; however, these conditions are just those for which the oscillation amplitude is small compared to the monotonic part, and thus we expect Eq. (2) to be an excellent approximation in these experiments. With the stated assumptions, Eq. (2) is seen to be valid for all components of the tensors $\tilde{\gamma}$ and $\tilde{\rho}$, and for arbitrary crystal orientation relative to $\vec{B}$. It is also appropriate for

the various harmonics, though for each harmonic n, X will be replaced by nX to give various values for α.

The arguments involving the thermoelectric coefficients are similar. It is convenient to work in terms of the thermoelectric tensor P defined via $\vec{E}=P\vec{U}$ rather than the usual thermopower S defined by $\vec{E}=S\vec{\nabla}T$. Experimentally, it is easier to measure $\vec{E}$ for fixed $\vec{U}$ rather than fixed $\vec{\nabla}T$, but other reasons will also be mentioned later.

The experimental condition $\vec{J}=0$ in Eq. (1) gives $\vec{E}=-\rho\epsilon''\vec{\nabla}T=\rho\epsilon''\gamma\vec{U}$ so that $P=\rho\epsilon''\gamma$. The main assumption to be made is that the dominant oscillatory term in $\rho\epsilon''$ is $\bar{\rho}\,\tilde{\epsilon}''$. The amplitude of the fundamental cannot be affected by $\tilde{\rho}\,\tilde{\epsilon}''$, but in general it seems reasonable to expect some harmonic enhancement in P from this term. We expect $\tilde{\rho}\,\bar{\epsilon}''$ to be a small contribution in the present work, though this may not be true in general. Introducing the Young result[1,2]

$$\tilde{\epsilon}''=\pm i\frac{\pi k}{e}\frac{D'(X)}{D(X)}\tilde{\sigma}=\beta\tilde{\sigma}\ ,$$

where $D'(X)=dD(X)/dX$, and the $\pm i$ is a phase factor appropriate to electron $(+)$ or hole $(-)$ orbits, respectively, then we have $\tilde{P}=\beta\bar{\rho}\tilde{\sigma}\gamma$. Using our earlier results, $\bar{\rho}\tilde{\sigma}=-\tilde{\rho}\sigma$ and $\gamma\simeq\rho/L_0T$, we find

$$P=-\frac{\beta}{L_0T}\tilde{\rho}\sigma\rho=-\frac{\beta}{L_0T}\tilde{\rho}\ . \tag{3}$$

We see that the tensors $\tilde{P}$ and $\tilde{\rho}$ should be essentially identical except for the constant $-(\beta/L_0)T=\mp i(3e/\pi kT)\times D'(X)/D(X)$. This is the obvious reason for using P rather than S. The final advantage of the use of P is that both $\tilde{P}$ and $\tilde{\rho}$ require exactly the same geometrical factors in their measurement; experimentally $\tilde{P}$ and $\tilde{\rho}$ are analogous except that the former uses a fixed heat current, the latter a fixed electric current. Again, Eq. (3) is valid for arbitrary crystal orientation and harmonic number.

III. EXPERIMENTS

The residual resistivity ratio of the sample that we have used is about 850(ρ273 K/ρ4.2 K), probably indicating an impurity level of about 100 ppm. There are many advantages in using a rather impure sample for this work, especially when previous experimental data for Al suggest that the relative amplitude of the oscillations in ρ_{xx} (as compared to the monotonic background) is only weakly dependent on purity. Thus an impure sample can provide larger absolute signal amplitudes and tends to reduce the harmonic content to manageable levels. We also note that the derivation in Sec. II assumes the validity of the Wiedemann-Franz law for the monotonic resistivities, i.e., $\bar{\rho}=\bar{\gamma}L_0T$. This implies a relatively impure sample, both to make sure that elastic scattering dominates, and also to avoid the effects of the lattice thermal conductivity λ_g that can become significant at high fields in pure samples (i.e., we need $\lambda''_{xx},\lambda''_{yy}\gg\lambda_g$ at all fields). An estimate of the effect of λ_g on $\bar{\gamma}$ may be made as follows. The largest change occurs in $\bar{\gamma}_{xx}$, which to lowest order[5] becomes $\bar{\gamma}_{xx}+\lambda_g\bar{\gamma}^2_{yx}$. Using $\bar{\gamma}_{yx}=\bar{\rho}_{yx}/L_0T=4.2\times10^{-3}\ (B/T)$ $\mathrm{W^{-1}\,m\,K}$ and[6] $\lambda_g=1.0\times10^{-2}\ \mathrm{T^2\,W\,m^{-1}\,K^{-1}}$, then $\lambda_g\bar{\gamma}^2_{yx}\sim1.1\times10^{-5}\ \mathrm{W^{-1}\,m\,K}$ at 8 T and is independent of T. The measured value of $\bar{\gamma}_{xx}$ is $\sim4\times10^{-3}/T\ \mathrm{W^{-1}\,m\,K}$ at 8 T and so the effect of λ_g is most significant at the highest temperature and is a 1% correction at 4 K and 8 T. We have ignored this contribution, but it is clear that the use of a sample with an order of magnitude higher resistivity ratio ($\sim10^4$) would necessitate a careful evaluation of the problem.

After spark machining, the sample was in the form of a flat plate with dimensions of approximately $25\times2.5\times1.5$ $\mathrm{mm^3}$. The sample faces were parallel to {001} planes to better than 1°. The damaged surface layer was removed by electropolishing and the crystal was soldered into the cryostat by using a commercial Al solder and flux. Two limbs spaced about 13 mm apart on the sample were used to attach the potential wires and carbon thermometers. All attachments were made with the same solder. Electrical currents were limited to 0.5 Å to minimize Lorentz forces; this was necessary because the cryostat was designed to allow some angular displacement on the sample (about 0.5° in any direction), and large Lorentz forces might well alter the sample axis slightly for the resistivity measurements. The available angular range is insufficient to investigate angular dependence but was useful in obtaining large oscillatory signals. Angular positions are not relevant to these experiments, but it was noted that the maximum amplitude could be obtained by tipping the crystal such that the field was about 0.5°–1° from [100] in a (001) plane: This is consistent with previous work.[3,4]

Carbon resistors monitored the temperature; suitable corrections were made for magnetic field dependence. It was found that $\bar{\rho}_{xx}=\bar{\gamma}_{xx}L_0T$ to within the experimental accuracy of (1–2)%, these checks were made at $B\lesssim3$ T where the oscillation amplitudes are small and do not interfere in the measurement. This provides a useful check on the overall calibrations, including the thermometry, as well as experimentally testing the major assumption required to obtain Eqs. (2) and (3). The magnetic field was produced by an 8 T superconducting solenoid, the small hysteresis due to a parallel superconducting switch being determined in separate experiments.

The measurements of the oscillatory quantities were made as follows. Because the phase and frequency of the oscillations are essentially independent of angle over the small range accessible to us, the magnetic field was fixed at a peak in the thermoelectric oscillatory output (the voltage output being monitored by a superconducting chopper amplifier) in the range 7–8 T, and the sample axis, was adjusted to give a large signal. Sweeps were then made to determine $\tilde{\rho}_{xx}$ with the sample in exchange gas; often this was done at 4.2 K to eliminate vibrational noise from the pumps since $\tilde{\rho}_{xx}$ provided only a small output signal for the maximum current of 0.5 A (see Fig. 1).

After evacuating the sample space and pumping the liquid helium to a suitable temperature, sweeps were made to record $\tilde{P}_{xx}$ and $\tilde{\gamma}_{xx}$. In the former case the same superconducting amplifier monitors the output, but in the latter case the recorded signal is the out-of-balance output from a bridge containing the two carbon resistors that monitor the temperature of the sample limbs. The use of such a carbon bridge introduces unavoidable nonlinearities into the measured signal. Carbon resistors have a rapidly changing sensitivity to temperature so that both the oscil-

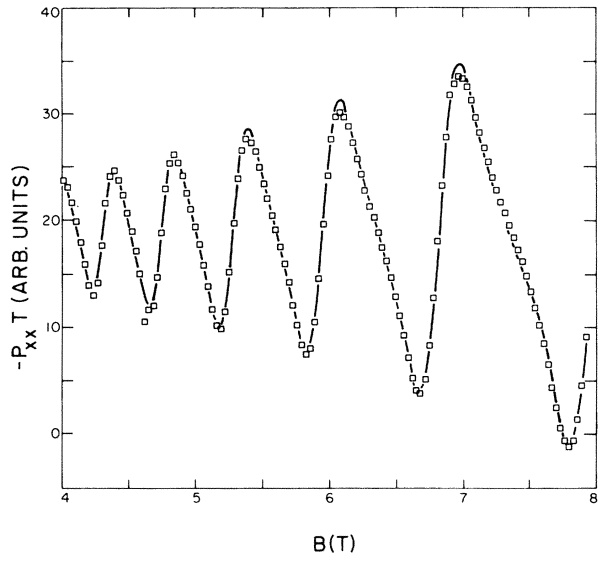

FIG. 1. Open squares are experimental data for $-\tilde{P}_{xx}$ as a function of B for run 5. The temperature varies from 3.094 to 3.127 K across this graph. The data may be converted to units of $A^{-1}mK$ by multiplying the ordinate scale by 2.76×10^{-9}; however, the zero is arbitrary, and in fact no monotonic part is visible in any of our data on P_{xx}. The solid line is a least-mean-squares computed fit using Eq. (6) of the text. The data have been inverted so that it resembles the thermopower $S_{xx}=-P_{xx}\gamma_{xx}$.

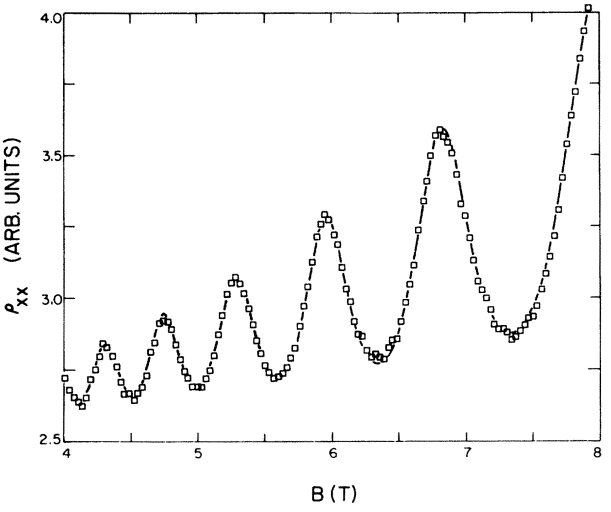

FIG. 2. Open squares are experimental data on the transverse resistivity ρ_{xx} at 4.20 K as a function of magnetic field B for run 5. The data may be converted to units of Ωm by multiplying the ordinate scale by 4.35×10^{-11}, but the zero is arbitrary. The solid line is a computed least-mean-squares fit using Eq. (7) of the text with a single free parameter A_1 (plus a low-order polynomial to account for the background). Since the observed value of A_1 is within 1% of the predicted value (see Table I, run 5) the fitted curve could be taken to be the theoretically predicted curve, given the data in Fig. 1 to fix all the free parameters as described in the text.

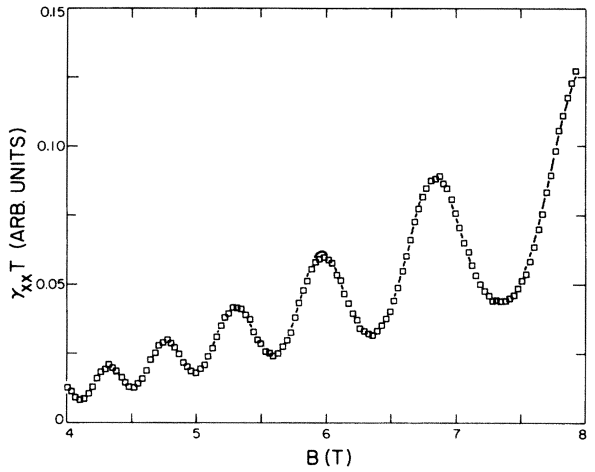

FIG. 3. Open squares are experimental data for $\gamma_{xx}T$ at about 3.2 K. The ordinate scales may be converted to $W^{-1}mK^2$ by multiplication by 0.0227. The solid curve is a computed least-mean-squares fit using Eq. (8) with a single free parameter E_1 (plus a low-order polynomial to account for the background). As with Fig. 2, the observed value of E_1 is within 2.5% of the predicted value (see Table I, run 5), and so the fitted curves could be taken to be the theoretically predicted curves with no free parameters.

lations in $\tilde{\gamma}$ and the monotonic background $\bar{\gamma}$ change the sensitivity appreciably as the field is swept. Some account of this is taken by evaluating the mean sensitivity for $\pm$ out-of-balance signals in the bridge at a number of fields and interpolating by means of simple polynomials. However, we have not corrected for nonlinearities in the bridge $\pm$ output at fixed field (these are not due to excessive bridge output, but reflect only sensitivity changes of the carbon resistors). Clearly $\tilde{P}_{xx}$ and $\tilde{\rho}_{xx}$ involve no such problems, and these coefficients can be compared with the minimum of experimental difficulty.

Output voltages were recorded both digitally and by x-y recorder during steady field sweeps, and Figs. 1–4 show typical digital recordings of the three coefficients. Most of the monotonic background is not displayed in the cases of ρ_{xx} and γ_{xx}, but for P_{xx} such a background was not visible. All of $\tilde{\rho}_{xx}$, $\tilde{P}_{xx}$, and $\tilde{\gamma}_{xx}$ were symmetric in B to high accuracy, i.e., the sign of B had no visible effect.

IV. ANALYSIS AND DISCUSSION

It soon became apparent that one of the major sources of error in this experiment is the accuracy with which the cyclotron mass m^* of the relevant orbit is known. Fortunately, it is possible to use the data on $\tilde{\gamma}$ to determine m^* reasonably accurately as was pointed out by Young.[2] The thermal damping factor $D''(X)$ appropriate to $\tilde{\gamma}$ passes through zero near $X=1.6$. Figure 5 shows a trace of $\tilde{\gamma}_{xx}$ over the field range where this occurs for $T\simeq3.6$ K together with $\tilde{\rho}_{xx}$ for comparison. The actual zero in $\tilde{\gamma}_{xx}$ tends to be obscured by harmonics (since the equivalent zero for the harmonics appears at higher fields) but least-mean-squares fits to the curves are found to be very sensitive to the value of m^*. The actual fitting was done as

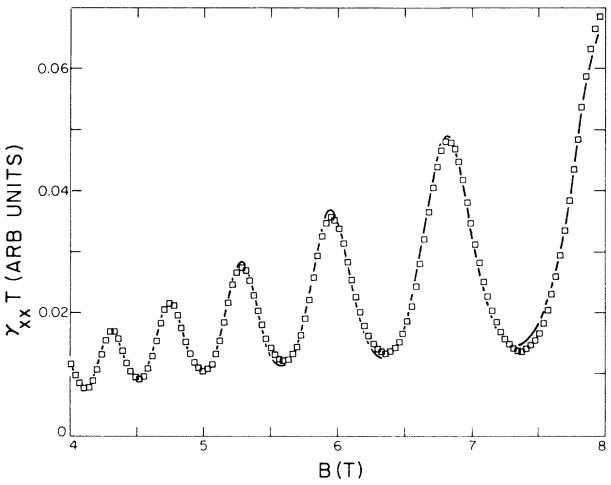

FIG. 4. Same as Fig. 3 but the data are taken at about 1.8 K. The ordinate may be converted to units of $W^{-1}\,m\,K^2$ by multiplication by 0.0389. The observed value of E_1 is within 1.5% of the predicted value (see Table I, run 5) and, as with Figs. 2 and 3, the fitted curve could be taken as the predicted curve. The changing form of the oscillation, being sinusoidal at high T (Fig. 3) and cusp shaped as low T as shown here, is automatically reproduced and results simply from variations in the thermal damping factors $D''(nX)$ on the various harmonics.

follows. First, $\tilde{\rho}_{xx}$ was used to fix some of the variables by approximating

$$\tilde{\rho}_{xx}=A_1 D(X)\exp\left[-\frac{B_1}{B}\right]\cos\left[\frac{2\pi f}{B}+\phi\right]. \tag{4}$$

The exponential term represents both a Dingle factor, usually written as $\exp(-2\pi^2 kT_D m^*/\hbar eB)$, which accounts for Landau-level broadening by impurity scattering, and a magnetic breakdown factor with the same functional dependence on B. Initially, an approximate value of m^*

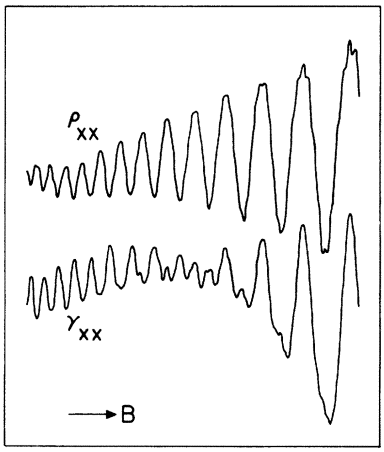

FIG. 5. Recorder traces of $\tilde{\rho}_{xx}$ and $\tilde{\gamma}_{xx}$ over the field range of 1.88–3.86 T at a temperature of about 3.4 K for $\tilde{\rho}_{xx}$ and 3.6 K for $\tilde{\gamma}_{xx}$. Near the center of the trace for $\tilde{\gamma}_{xx}$, the thermal damping factor $D''(X)$ changes sign, which causes a phase inversion of $\tilde{\gamma}_{xx}$ compared to $\tilde{\rho}_{xx}$. The presence of a strong second-harmonic component obscures the precise crossover point.

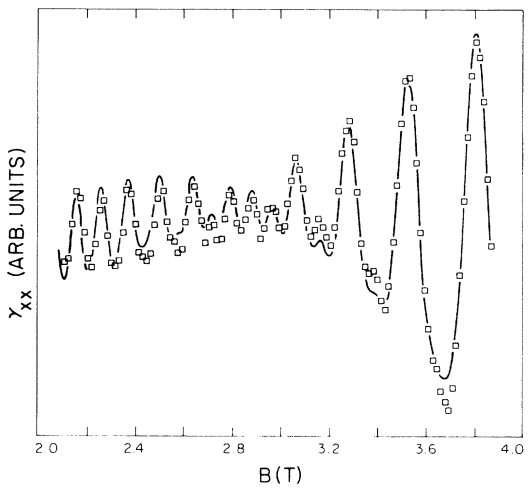

FIG. 6. Points are a digital recording of the same data as shown in Fig. 5 on $\tilde{\gamma}_{xx}$. The solid curve is a least-mean-squares computed fit using Eq. (5) of the text (plus a monotonic contribution).

was used to evaluate $D(X)$ as a function of B. Having obtained values for B_1, f, and ϕ, $\tilde{\gamma}_{xx}$ was then fitted using

$$\tilde{\gamma}_{xx}=\sum_{n=1}^{2} E_n D''(X)\exp\left[-\frac{B_n}{B}\right]\cos\left[n\left[\frac{2\pi f}{B}+\phi\right]\right] \tag{5}$$

with variables E_1, E_2, B_2, and m^*; n refers to the harmonic number. The form of the phase factors, i.e., $n\phi$, was suggested by visual examination of this and other data and has been used throughout the analysis. It leads to a pronounced cusp shape of the waveform for $\tilde{\rho}_{xx}$ (and $\tilde{\gamma}_{xx}$ at low T) at high fields, cf. Figs. 2 and 4. The fit is very sensitive to m^*; an example of the fitted curve is shown in Fig. 6. Although another iteration was carried out using this new m^* in Eqs. (4) and (5), again no significant change resulted. The final value was found to be $m^*=0.0867m_e$ with the repeatability suggesting an accuracy of 1%. The previous literature values[7,8] are $0.102\pm0.006m_e$ and $0.093\pm0.010m_e$.

The remaining data were analyzed over the range 4–8 T. Because the signal-to-noise ratio is usually very high for the thermoelectric oscillations, $\tilde{P}_{xx}$ was always fitted first. It was assumed that this coefficient can be approximated by a series of the form

$$\tilde{P}_{xx}T=\sum_{n} C_n D'(nX)\exp\left[-\frac{B_n}{B}\right]\sin\left[n\left[\frac{2\pi f}{B}+\phi\right]\right], \tag{6}$$

with the variables being the coefficients C_n, B_n, f, and ϕ. Because the temperature of the sample changed during a field sweep, simple linear interpolations were used to find T on a point-by-point basis so that $\tilde{P}_{xx}T$ and nX could be evaluated with no appreciable error. Extending the series to $n=3$ provided an adequate fit to all data; Fig. 1 shows a typical example. It was usually necessary to include a contribution of the form $a+bB$ to account for the monotonic background. The frequency f was always in the

range 46.8±0.2 T for all the data and is in excellent agreement with previous work.[9] The coefficients B_n increased systematically with n and were typically 14 T for the fundamental. However, it was found that B_1 in particular depends on B and has decreased to about 7 T by fields of ~ 3 T. Thus the exponential terms in Eq. (6) do not provide an exact representation of the amplitude field dependence, but their use should simply be viewed as a procedure to obtain a reasonable fit to the data and, providing the same form is also used for $\tilde{\rho}_{xx}$ and $\tilde{\gamma}_{xx}$, we do not expect this to have any significant effect on our final results. We might also mention that the B_n depends strongly on angle, and for $\vec{B}$ parallel to [001], B_1 drops to about 8 T for B in the range 4–8 T. However, we have not made a systematic study of this, and in general, the precise orientation of our sample in the various experimental runs is not known.

Once we had an acceptable fit to $\tilde{P}_{xx}T$, the following expressions were used to represent $\tilde{\rho}_{xx}$ and $\tilde{\gamma}_{xx}$:

$$\tilde{\rho}_{xx}=\sum_n A_1\left[\frac{C_n}{C_1}\right]D(nX)\exp\left[-\frac{B_n}{B}\right]\times\cos\left[n\left[\frac{2\pi f}{B}+\phi\right]\right], \tag{7}$$

$$\tilde{\gamma}_{xx}T=\sum_n E_1\left[\frac{C_n}{C_1}\right]D''(nX)\exp\left[-\frac{B_n}{B}\right]\times\cos\left[n\left[\frac{2\pi f}{B}+\phi\right]\right]. \tag{8}$$

The coefficients C_n, B_n, f, and, in the first instance, ϕ, were taken directly from the results on $\tilde{P}_{xx}T$. Each of Eqs. (7) and (8) contain only one variable, A_1 or E_1, though in practice it was always necessary to include monotonic contributions, usually up to a term in B^2. Figures 2–4 show examples of the fitted curves to the experimental points, and it is clear that the agreement is excellent on all respects. In particular, the cusp-shaped waveform for $\tilde{\rho}_{xx}$ is well reproduced. This same waveform is observed for $\tilde{\gamma}_{xx}$ at low temperature (Fig. 4), but it becomes much more sinusoidal at higher temperatures (Fig. 3); this arises simply from the fact that at high T (i.e., ~ 3.5 K), $D''(2X)$ has a zero in the midrange of the data, so the second-harmonic contribution disappears. The characteristic cusp shape for $\tilde{\rho}_{xx}$ and $\tilde{\gamma}_{xx}$ and the triangular shape for $\tilde{P}_{xx}$ result from the form of the phase locking of the harmonics in Eqs. (6)–(8), together with the overall phase shift of $\pi/2$ predicted to occur for $\tilde{P}_{xx}$ relative to the resistivities. Incidentally, the sign of the phase shift indicates that the orbit we are observing is electron-like as expected. In a number of cases ϕ was made a variable in Eqs. (7) and (8). However, the best value as determined by least-mean-squares fitting was always very close to that obtained from Eq. (6); in the worst case, the discrepancy was 5°, but in the majority of cases the same phases were obtained to within 2°. In other words, the expected identical phases of $\tilde{\rho}_{xx}$ and $\tilde{\gamma}_{xx}$ and the phase shift of $\tilde{P}_{xx}$ by $\pi/2$ are observed to be correct to a precision of about 2°.

The sensitivity of the C_n and B_n to sample orientation means that all the coefficients $\tilde{P}_{xx}$, $\tilde{\gamma}_{xx}$, and $\tilde{\rho}_{xx}$ must be obtained at the same angle, so it was always essential to obtain all sets of data in each experiment. On the other hand, the actual temperature at which any individual data set is measured is not particularly important since all thermal effects are taken into account in the thermal damping factors $D(X)$, $D'(X)$, and $D''(X)$.

According to Eqs. (2) and (3) the amplitudes of the oscillatory components are all related via known factors. These equations apply to each harmonic, but it will be seen from the way that the data have been treated that we essentially fit all harmonics simultaneously, so we are left with only three coefficients to compare, i.e., A_1, C_1, and E_1. The predicted ratios are $(C_1/A_1)=3e/\pi k$ and $E_1/A_1=-3/L_0$. Table I presents all the experimental results in the form $(C_1/A_1)(\pi k/3e)$ and $-(E_1/A_1)(L_0/3)$, and it will be observed that they are in good agreement with the expected values of unity. The consistency of the results for (C_1/A_1) is traceable to the fact that there are essentially no difficult calibrations involved in the fitting procedures. The same amplifiers and filters are used to record the data, the differences being the use of a heat current for $\tilde{P}_{xx}$, and an electric current for $\tilde{\rho}_{xx}$ (both of which are easily measured to 0.1%), and the requirement of T in the former case (which is unlikely to be in error by more than 10 mK. On the other hand, the determination of E_1 requires not only T, but also the oscillatory temperature difference across the sample. As we have indicated in Sec. III, the problems have only partially been overcome,

TABLE I. Observed values of the reduced coefficients $(C_1/A_1)(\pi k/3e)$ and $-(E_1/A_1)(L_0/3)$, both of which should be unity according to theory.

Run	$(C_1/A_1)(\pi k/3e)$	$-(E_1/A_1)(L_0/3)$	Approx. T (K)[a]
1	0.993	0.946	3.6
2	1.022	1.070	2.5
3	1.006	1.090	1.8
4	0.985	1.076	3.1
5[b]	1.002	1.024	3.2
		0.987	1.8
Mean values	1.002±0.014	1.02±0.05	

[a]The temperatures are usually different for $\tilde{\rho}_{xx}$ as compared to $\tilde{\gamma}_{xx}$ and $\tilde{P}_{xx}$. This table gives the approximate T relevant to $\tilde{\gamma}_{xx}$ and $\tilde{P}_{xx}$ because $\tilde{\rho}_{xx}$ is insensitive to T.

[b]$\tilde{\rho}_{xx}$ and $\tilde{\gamma}_{xx}$ were measured at two temperatures. The observed values of A_1 were identical to within 0.5% for data taken on $\tilde{\rho}_{xx}$ at 1.40 and 4.2 K; the mean was used in the analysis.

and the residual errors in E_1 ($\sim\pm5\%$) are not unexpected.

The only other uncertainty that will appear in our final results is that arising from m^*. By repeating one series of fits with m^* increased by 2%, we found that C_1/A_1 was decreased by 3%; a similar analysis was not carried out for E_1/A_1, but we would expect a similar change. Assuming the uncertainty in m^* to be $\pm1\%$, then our final value for $(C_1/A_1)(\pi k/3e)$ is 1.002 ± 0.030, and for $-(E_1/A_1)(L_0/3)$ it is 1.02 ± 0.07.

The obvious result of this work is that, given any one of the oscillatory components $\tilde{\rho}_{xx}$, $\tilde{\gamma}_{xx}$, or $\tilde{P}_{xx}$ for Al, the others can be predicted to high accuracy in all detail by the use of Eqs. (2) and (3). The fitted curves in Figs. 2–4 could be considered to be theoretically predicted curves since the predicted and measured amplitudes are the same to within experimental error. This conclusion means that each transport component contains essentially all the useful information (except for the electronlike or holelike character of the orbit, which requires a comparison of $\tilde{P}_{xx}$ with either of the others) and one should use whichever is convenient for a particular application. Because these experiments have investigated only a single component of the tensors $\tilde{\rho}$, $\tilde{\gamma}$, and $\tilde{P}$, it is premature to claim that all components are so well behaved. Nevertheless, with the assumption that $\bar{\rho}=\bar{\gamma}L_0T$, Eqs. (2) and (3) should apply to any metal crystal at any orientation relative to $\vec{B}$, e.g., a previous study of the quantum oscillatory effects in the thermopower of Mo[9] can now be considered to be a study of the effects of the resistivities for all intents and purposes.

As pointed out by Streda and Vasek,[10] the verification of Eq. (3) can be considered to be a verification of the closely related Mott relationship $S=L_0eT(d\ln\rho/d\epsilon)_\mu$: Although this equation has been in use over a long period of time, it has not been subject to experimental tests until very recently. In retrospect, it is not completely clear why the relationship is directly applicable in the present case. It has been established that the monotonic part of the Nernst-Ettingshausen coefficient $\bar{P}_{yx}$ obeys the appropriate Mott relationship very accurately[11] provided that a many-body enhancement factor is included in the calculation (Ref. 11 uses the notation P^a for $\bar{P}_{yx}$). In this case $\bar{P}_{yx}$ depends only on the density of electronic states $N(\mu)$ evaluated at the chemical potential μ. Both experiment and theory[12–14] agree that the appropriate $N(\mu)$ is that enhanced by many-body effects. In the present theory, there is no explicit reference to an enhancement factor. It may be that the use of the experimental m^*, which is enhanced, has implicitly included the effect. In the high-field limit ($X\to0$), Eq. (3) reduces to $\tilde{\epsilon}''=\pm i(\pi k/e)(X/3)\tilde{\sigma}$, where X contains the enhanced m^*. However, as $B\to0$ ($X\to\infty$), Eq. (3) becomes $\tilde{\epsilon}''=\pm i(\pi k/e)\tilde{\sigma}$, which is independent of m^*. This might suggest that the enhancement is only relevant when the structure in the density of states is coarser than kT in scale, but a clarification of this problem must be left to theorists.

Finally, we note that Eqs. (2) and (3) contain no explicit reference to phonon drag, and we, therefore, conclude that phonon drag plays a negligible role in the quantum oscillatory effects in Al. This is perhaps not unexpected, but it is, nevertheless, useful to have experimental data confirming this conclusion.

V. CONCLUSIONS

These experiments demonstrate that, at least for the case of Al, the oscillatory components in the transverse electrical and thermal resistivities, as well as those in the thermopower, are all intimately related by known equations. Given any one oscillatory component, the others are readily calculated at any field or temperature. Although the oscillations in the thermopower are very large and perhaps the most easily accessible experimentally, those in the thermal resistivity have the merit of good signal to noise at low temperatures and also have the useful feature that the effective mass of the orbit can be obtained very accurately from a single field sweep, providing the zero in the amplitude is observable.

The precise way in which the many-body enhancement effects are accounted for in the calculation has not been resolved, though from an experimental point of view this is clearly not a problem since the expressions we have used certainly fit the experimental results very accurately. Finally, we conclude that phonon drag plays no observable role in the mechanism producing quantum oscillations in the transport properties of Al.

ACKNOWLEDGMENTS

I appreciate conversations with Dr. E. Zaremba. The help of Mr. P. Riley in preparing the sample is also gratefully acknowledged. This work has been supported by the Natural Science and Engineering Research Council of Canada.

[1]R. Fletcher, J. Low. Temp. Phys. 43, 363 (1981).
[2]R. C. Young, J. Phys. F 3, 721 (1973).
[3]H. Sato, K. Shimiza, and K. Yonemitsu, J. Low Temp. Phys. 35, 41 (1979).
[4]W. Kesternich and C. Papastaikoudis, J. Phys. F 7, 837 (1977).
[5]R. Fletcher, J. Phys. F 4, 1155 (1974).
[6]H. N. De Lang, H. van Kempen, and P. Wyder, J. Phys. F 8, L39 (1978).
[7]C. O. Larson and W. L. Gordon, Phys. Rev. 156, 703 (1967).
[8]B. J. Thaler and J. Bass, J. Phys. F 5, 1554 (1975).
[9]R. Fletcher, Can. J. Phys. 60, 122 (1982).
[10]P. Streda and P. Vasek, Phys. Status Solidi B 103, K137 (1981).
[11]B. J. Thaler, R. Fletcher, and J. Bass, J. Phys. F 8, 131 (1978).
[12]J. L. Opsal, B. J. Thaler, and J. Bass, Phys. Rev. Lett. 39, 363 (1977).
[13]S. K. Lyo, Phys. Rev. B 17, 2545 (1978).
[14]Y. A. Ono and P. L. Taylor, Phys. Rev. B 22, 1109 (1980).